Mathematical Biosciences and Engineering

MBE, 19(9): 9168–9199.
DOI: 10.3934/mbe.2022426
Received: 15 March 2022
Revised: 01 June 2022
Accepted: 05 June 2022
Published: 22 June 2022

http://www.aimspress.com/journal/MBE

Research article

Next-generation 5G fusion-based intelligent health-monitoring platform for ethylene cracking furnace tube

Delong Cui[1], Hong Huang[1], Zhiping Peng[1,2,*], Qirui Li[1], Jieguang He[1], Jinbo Qiu[1], Xinlong Luo[1], Jiangtao Ou[3] and Chengyuan Fan[3]

[1] College of Electronic Information Engineer, Guangdong University of Petrochemical Technology, Maoming, China
[2] Jiangmen Polytechnic, China
[3] AI Sensing Technology, Chancheng District, Foshan, China

* **Correspondence:** Email: zhipingpeng@gdupt.edu.cn.

Abstract: This study aimed to develop a 5G + "mixed computing" + deep learning-based next-generation intelligent health-monitoring platform for an ethylene cracking furnace tube based on 5G communication technology, with the goal of improving the health management level of the key component of ethylene production, that is, the cracking furnace tube, and focusing on the key common technical difficulties of ethylene production of tube outer-surface temperature sensing and tube slagging diagnosis. It also integrated the edge-fog-cloud "mixed computing" technology and deep learning technology in artificial intelligence, which had a higher degree in the research and development of automation and intelligence, and was more versatile in an industrial environment. The platform included a 5G-based tube intelligent temperature-measuring device, a 5G-based intelligent peep door gearing, a 5G-based edge-fog-cloud collaboration mechanism, and a mixed deep learning-related application. The platform enhanced the automation and intelligence of the enterprise, which could not only promote the quality and efficiency of the enterprise but also protect the safe operation of the cracking furnace device and lead the technological progress and transformation and upgrading of the industry through the application.

Keywords: 5G fusion; intelligent health-monitoring; ethylene cracking furnace tube; edge-fog-cloud collaboration mechanism; deep learning technology

1. Introduction

Manufacturing industries play a key role at the national level and even in the whole human society [1]. Intelligent manufacturing is a major trend and the core content of the current manufacturing development. It is also an important initiative to accelerate the change in the development mode and promote the industry to the middle and high ends [2]. However, in intelligent manufacturing, the real-time communication between cloud platform and factory production facilities, information interaction between massive sensors and artificial intelligence platform, and efficient interaction between human and machine have diverse demands on communication networks and performance requirements, necessitating the introduction of highly reliable wireless communication technologies [3]. 5G network can provide extremely low time delay, high reliability, and massive connectivity, causing a new change to intelligent manufacturing systems [4,5].

In the petrochemical industry, the ethylene industry is particularly important. The industry chain covers a wide range. The current global production of ethylene continues to increase at a high rate of 7–8% per year [6]. The ethylene cracking furnace is the most important device in the ethylene industry. Further, the tube is the most critical part of the ethylene cracking furnace and also the reactor of steam cracking [7]. When the raw materials undergo cracking reactions at high temperatures, coke particles or coke bodies are generated and attached to the surface of tubes and equipment due to the special characteristics of hydrocarbons. Therefore, coke is inevitably generated during the cracking of hydrocarbon feedstocks, and the thickness of the coke layer increases further with the increase in the cracking time. The coke formed under such high-temperature conditions is a poor conductor of heat, which reduces the heat transfer coefficient, increases energy consumption, increases the thermal resistance of the tube wall, leads to a smaller inner diameter of the tube and a higher outer-surface temperature, and even blocks the tube, thus affecting the stable operation of the device. A more negative effect is the carburization of the tube, which causes material deterioration and reduces the mechanical strength of the tube [8]. Slagging leads to frequent coke cleaning of the cracking furnace, shortening of the cracking furnace operation and the effective production time of the device, an increase in energy consumption and equipment damage, and a decrease in tube life. Further, tubes are usually made of the nickel-chromium alloy and are expensive. Therefore, tube slagging causes a sharp increase in the production cost of ethylene devices. Additionally, severe slagging can lead to tube blockage and even tube explosion, forcing the ethylene production device to stop. If the local overtemperature caused by tube fire and internal slagging is not detected in time, it may result in a great safety hazard. In serious cases, it may even burn through the tube and cause a fire in the furnace, resulting in serious economic losses, endangering operators' lives, and bringing huge economic losses and safety risks to the petrochemical industry.

It is of great significance to conduct the diagnosis and prediction of tube slagging degree accurately and extend the effective operating cycle of the tube safely. These are effective technical means to ensure the safety of cracking furnace operation and improve the production efficiency of cracking furnace tubes.

2. Related work

2.1. Outer-surface temperature measurement and slagging detection of the ethylene cracking furnace tube

Cracking overtemperature is the most important cause of slagging in cracking furnace tubes, which, in turn, leads to mechanical failure of the tube [9]. Therefore, monitoring of the cracking furnace tube temperature during the ethylene production process, especially the outer-surface temperature monitoring, is of great importance, and then the tube slagging situation needs to be examined and judged [10–12].

At present, the outer-surface temperature of the cracking furnace tube is mainly measured by two methods [13,14]. First, the thermocouple measurement is performed in different parts of the tube. Second, the outside operator is arranged for tube positioning and measurement by aiming at the tube with the thermoprobe through the cracking furnace peephole regularly. The tube outer-surface temperature is measured using an artificial thermoprobe as shown in Figure 1 [15]. However, both methods have serious limitations: the thermocouple method is readily exposed to a temperature shift owing to the high-temperature environment in the furnace, resulting in extreme challenges in the process operation and control. Also, the portable thermoprobe has the following drawbacks that hinder ethylene production: 1) the large cracking furnace smoke and fire, high temperature, and large heat radiation result in high temperature in the surrounding environment. This is coupled with the cracking furnace constantly vibrating and generating noise, harsh temperature measurement environment, and high labor intensity. Especially, the current cracking furnace external operators are significantly reduced. Reducing their labor intensity is highly important to improve the quality of labor and labor enthusiasm [16]. 2) Cracking furnace is usually equipped with several hundreds of tubes. However, the manpower and time are limited due to the low efficiency of manual temperature measurement. Hence, the external operator can usually only randomly select a small number of tubes for temperature measurement. Further, the measured temperature data are not uniform, incomplete, and therefore not representative [17]. 3) The infrared beam angle of incidence has a greater impact on the infrared temperature measurement accuracy. Usually, the vertical irradiation accuracy is the highest, but the handheld approach is more arbitrary. Therefore, the manual temperature measurement accuracy is low, coupled with different operating habits, resulting in the same tube having 20–30℃ deviation in the measurement results [18]. 4) Cracking furnaces often shake in the production process. The visual inspection of the tube position and then hand aiming greatly affect the temperature measurement accuracy of the tube [19]. A few ethylene production enterprises use an infrared thermal imager and a multispectral monitoring probe for temperature measurement on the outer surface, as shown in Figure 2. Nevertheless, both methods are costly and uncontrollable, limiting their wide application. Therefore, many ethylene production enterprises urgently need a cost-effective, real-time online automatic monitoring of the outer-surface temperature of the cracking furnace tube with accurate diagnosis and prediction of the tube slagging platform.

Figure 1. Measurement of the outer-surface temperature using a thermoprobe.

Figure 2. Measurement of the outer-surface temperature using a multispectral probe.

2.2. Problems and challenges

Based on the aforementioned common needs of ethylene production enterprises, this study developed an intelligent health-monitoring platform for ethylene cracking furnace tubes, which was successfully applied and achieved expected results [21,22]. Although the platform could effectively achieve the intelligent monitoring of cracking furnace tubes, tube monitoring became more difficult with the development of large, complex, and extreme operating parameters of cracking furnace equipment. The platform still had some technical difficulties that needed to be solved. The main aspects were as follows:

1) LoRa network is easy to build and deploy. It has the advantages of low power consumption, long transmission distance, license-free band nodes, and long battery life. However, it also has the disadvantages of spectrum interference, highly centralized technology, need for new networks, low transmission rate, and small transmission bandwidth. Also, it is not suitable for video transmission, making it difficult to expand the scale of monitoring. Further, it has limited transmission data volume and high site distribution environment requirements, which is not conducive to the promotion and application of this platform.

2) Temperature measurement using an intelligent temperature-measuring device still requires the external operator to open the peep door manually and control the temperature-measuring device

by remote control to scan the outer surface of the tube and the inner wall of the furnace wall, resulting in manual intervention in the entire temperature measurement process and hence limiting its working efficiency. Therefore, intelligent modification of the peep door and temperature-measuring device is urgently required.

3) The platform uses a traditional central cloud structure, where the sampled data from devices are transmitted to a remote cloud for centralized analysis and processing. This has problems such as computing latency, congestion, low reliability, and security attacks.

4) The core indicators of the intelligent temperature-measuring device, such as intelligence, cost-effectiveness, accuracy, measurement time, equipment cost, installation and maintenance cost, and data transmission, have obvious advantages compared with similar products at home and abroad. However, the intelligent algorithms in the temperature-measuring device, such as overlapping tube identification, surface temperature and inner-wall temperature identification, and tube outer-surface temperature measurement, are cured in the embedded chip of the instrument, which lacks self-adaptation to the field monitoring environment. As a typical edge device, the intelligent temperature-measuring device does not take full advantage of the edge-cloud collaboration for self-directed learning.

Recently, modern communication technology represented by 5G; computer technology represented by edge computing, fog computing, and cloud computing; and artificial intelligence technology represented by deep learning have developed rapidly and are the hot spots for research and application in industry and academia in recent years. We used the interconnectivity and powerful communication capability of 5G and integrated edge-fog-cloud mixed computing and deep learning technology to build a 5G + mixed computing + deep learning technology system. The objectives were to upgrade and optimize the ethylene intelligent health-monitoring platform for the cracking furnace tube under cloud computing environment, solve the technical problems of the platform, improve the intelligence and automation of the platform, create the next-generation intelligent health-monitoring platform for ethylene cracking furnace tubes, further promote the quality and efficiency of the enterprise, and better protect the safe operation of the cracking furnace device.

3. 5G fusion-based next-generation intelligent health-monitoring platform for the ethylene cracking furnace tube

3.1. Overall structure of the proposed platform

Figure 3 illustrates the overall structure of the proposed 5G fusion-based next-generation intelligent health-monitoring platform for the ethylene cracking furnace tube. Studying the key common problems in the platform, such as 5G-based intelligent temperature-measuring device, 5G-based intelligent peep door gearing, 5G-based edge-fog-cloud collaboration mechanism, and mixed deep learning application, can improve the overall performance of the platform, enhance the automation and intelligence level of the platform, further promote the quality and efficiency of the enterprise, and better protect the safe operation of the cracking furnace device [23,24].

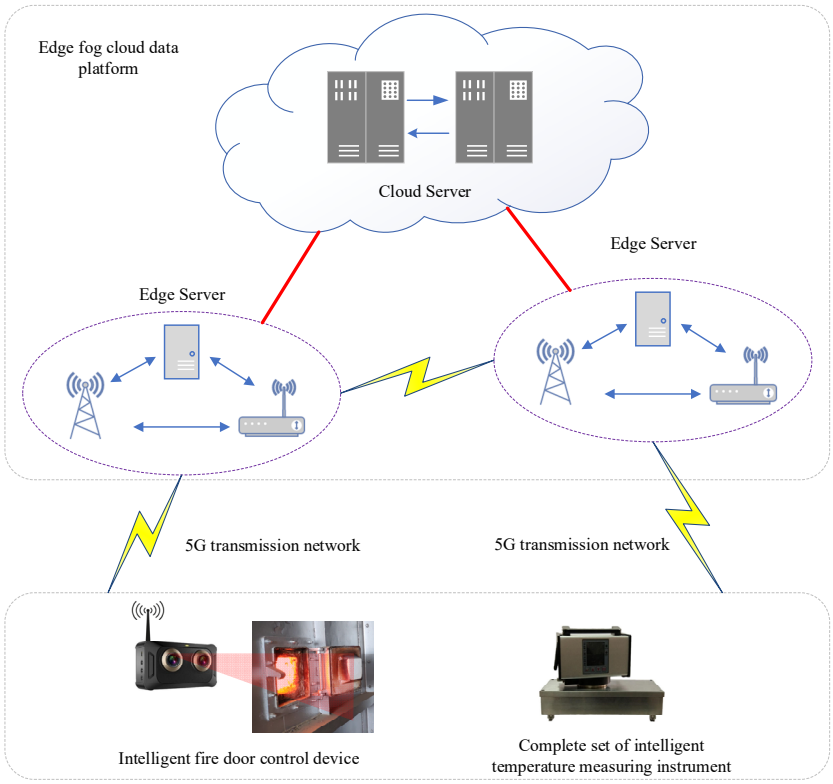

Figure 3. Next-generation 5G fusion–based intelligent health-monitoring platform.

3.2. Platform composition and technical solutions

3.2.1. 5G-based intelligent temperature-measuring device

The 5G-based intelligent temperature-measuring device comprises an intelligent temperature-measuring device, a drive console, and a charging protection cabin.

1) Overall structure of the intelligent temperature-measuring device

The intelligent temperature-measuring device is mainly applied to the intelligent monitoring of tube outer-surface temperature, cracking furnace peep-hole initial operating parameters of adaptive matching, and cracking furnace peephole operating conditions of real-time video monitoring. It also aims to achieve remote automatic measurement of the cracking furnace tube and remote monitoring of the cracking furnace peep door, solve the measurement deviation caused by the operator's technical level and operation method in the manual temperature measurement process, reduce operator’s labor intensity, and improve the accuracy and timeliness of data measurement and processing analysis. Figure 4 shows the overall structure of the intelligent temperature-measuring device. It comprises the main body control board, an infrared temperature sensor, a laser distance sensor, an HD binocular camera, the 5G wireless communication module, and the stepper motor drive module.

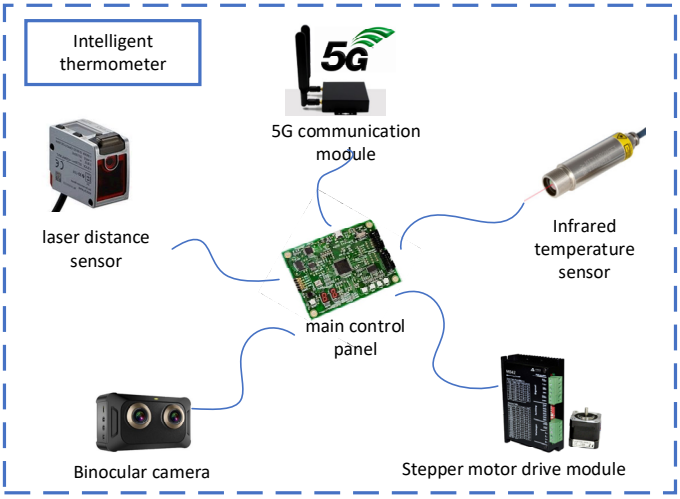

Figure 4. Intelligent temperature-measuring device.

2) Overall structure of the drive console

The drive console is the main part of intelligent temperature-measuring device motion control, mainly used to realize intelligent motion control of the intelligent temperature-measuring device. Figure 5 shows the overall structure of a drive console, which comprises a high-precision electric turntable, two-phase hybrid stepper motors, magnetic charging modules, Hall sensors, and optoelectronic sensors. Through the cooperation of each module, the functions of starting position positioning, initial angle determination, horizontal linear motion, simultaneous rotation of the measurement angle during automatic temperature measurement using an intelligent temperature-measuring device, as well as the function of self-testing and automatic recharging of the instrument after the measurement, can be realized.

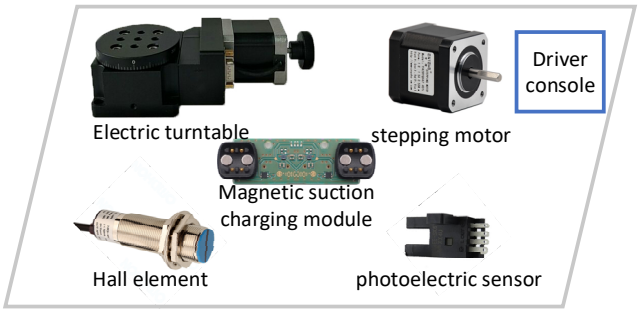

Figure 5. Drive console.

3) Overall structure of the charging protection cabin

The intelligent temperature-measuring device also comprises a charging protection cabin, as shown in Figure 6. It comprises an in-cabin inspection site, the power display section, and the magnetic charging module. During the automatic measurement process of the intelligent temperature-measuring device, when the power battery runs low, the automatic return to the charging protection cabin is initiated to realize the automatic charging of the temperature-measuring device. The in-cabin inspection site in the charging cabin is used to realize the in-cabin inspection function

of the intelligent temperature-measuring device. Whenever the intelligent temperature-measuring device measurement task is completed, the instrument automatically returns to the cabin, the detection point detects that the instrument has entered the cabin completely, and the charging protection cabin automatically locks the protection cabin door to prevent accidental loss of the instrument.

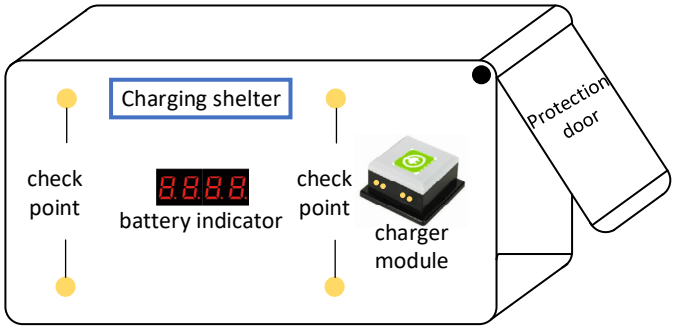

Figure 6. Intelligent temperature-measuring device: charging protection cabin.

3.2.2. Development of 5G-based intelligent peep door gearing

The ethylene cracking furnace is closed all year-round to minimize the heat loss from the furnace. The only way to measure the temperature on the outside of the cracking furnace tube is to make the cracking furnace tube visible to the temperature-measuring device through a small peephole in the furnace wall. Owing to technical limitations and safety, peep doors are still used mechanically and manually, which directly affects the automation and intelligence of the tube temperature measurement.

The small peephole is the only way for the intelligent temperature-measuring device to peek into the cracking furnace and perform an outer-surface temperature measurement. The temperature-measuring device requires a high degree of a peep door opening. If the peep door is not open enough, some of the cracking furnace tubes may not be scanned and the detection data may be incomplete.

1) Opening and closing gearing of the peep door

The peephole of the ethylene cracking furnace is mechanically a vertical rotating single door. As shown in Figure 7, high-temperature and high-pressure flames are present in the ethylene cracking furnace chamber. When the peep door is opened, the high-temperature heat is radiated outward through the peephole due to the negative pressure effect. Therefore, the start/stop control of existing peep doors is opened by conventional manual operation. The inspection workers must wear high-temperature protective clothing, goggles, gloves, and other facilities before they can peep inside the furnace. The high-temperature and harsh operating environment bring great labor intensity to inspection workers and even causes injuries.

Automatic opening/closing control of peep doors is achieved using a chain-type electrical system/drive. The peep door gearing consists of a stepper motor, a bi-directional drive telescopic chain, a connecting bracket, and a peephole door connector.

The peep door gearing is located under the peep door, suspending the connection with the cracking furnace, reducing the direct contact area with the cracking furnace, effectively decreasing the operating environment temperature, reducing the high-temperature wear of the peep door gearing,

and increasing its service life.

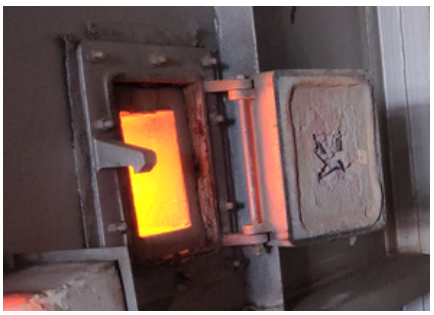

Figure 7. Site image of the peephole of the ethylene cracking furnace.

2) Peep door position detection device

The amplitude of the peep door opening is one of the main bases for determining the scanning position and scanning initialization angle of the intelligent temperature-measuring device. It is directly related to the accuracy of tube temperature measurement and the prediction of tube operation status. Meanwhile, when the automatic control of peep door opening and closing is realized, the telescopic chain of peep door gearing is beyond the working position and damaged if the position of peep door operation is not detected in real time. This is because the motor cannot be controlled and stops. Therefore, the accurate detection of the peep door position is one of the key issues to be solved.

The peep door position information is detected by the spring-press conversion method to ensure the accurate identification of the peep door position state. As shown in Figure 8, the spring is connected to the peep door through a bracket, and the other end of the spring is connected to the pressure sensor. When the position of the peep door changes, it drives the spring to deformation. The spring force is used to squeeze the pressure sensor to generate voltage change, the voltage change data are collected from the pressure sensor, the relationship between voltage and position is analyzed, and the position of the peep door is indirectly measured.

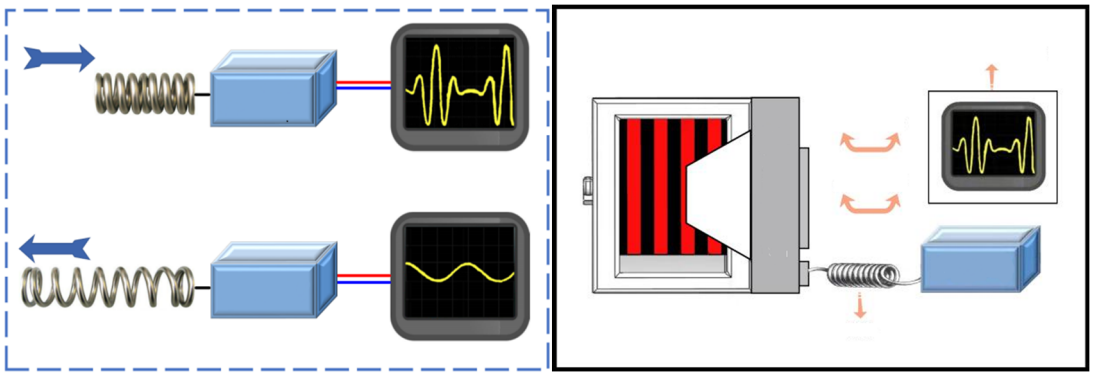

Figure 8. Design principle of the peep door position detection device.

3.2.3. 5G-based edge-fog-cloud collaboration mechanism

Edge computing, fog computing, and cloud computing are core supporting technologies of the

intelligent monitoring platform structure [25]. Edge computing provides edge intelligent services nearby to meet the critical needs of industry digitization for agile connectivity, real-time business, data optimization, application intelligence, security, and privacy protection. Fog computing extends the services and tasks of the cloud to the network edge. Cloud computing, with its resource advantages, can provide large-scale data storage, analysis, working, and processing capabilities. At present, the cloud computing service model aggregates computation in the central cloud, which has shortcomings in location awareness, real-time content delivery, service latency, and mobility support [26,27].

1) Edge-fog-cloud layering mechanism

Based on the central cloud structure, a three-tier architecture system of mixed computing based on edge computing, fog computing, and cloud computing was built, as shown in Figure 9. The 5G fusion-based next-generation intelligent monitoring platform for the ethylene cracking furnace tube comprises an edge computing layer, a fog computing layer, and a cloud computing layer. The edge computing layer communicates with the fog computing layer over a 5G network, while the fog and cloud computing layers are connected over a dedicated high-speed wired network.

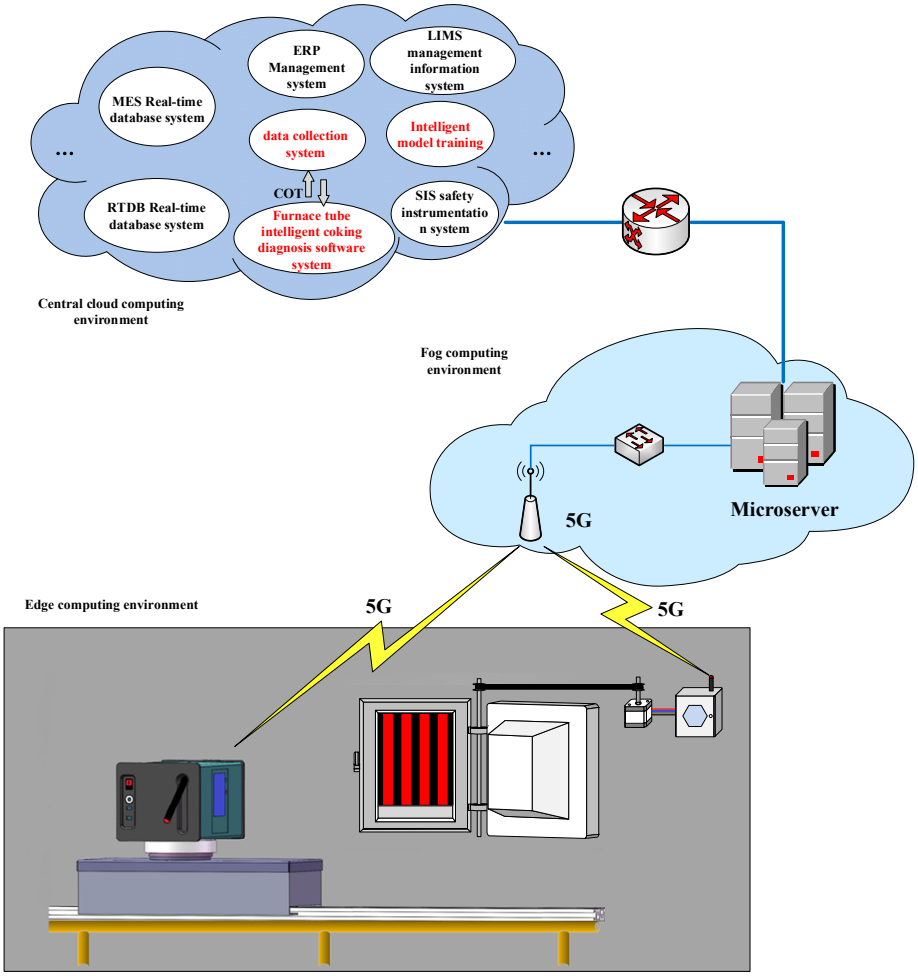

Figure 9. Three-layer structure of the intelligent monitoring platform.

Edge computing layer: It mainly includes an intelligent temperature-measuring device and an

intelligent peep door gearing, which can collect tube surface temperature data and peep door status data. The tube surface temperature data acquisition is complex, requiring optimization of the initial position and angle of temperature measurement, dual-phase synchronized control of horizontal motion and running rotation, overlapping tube identification, identification of outer-surface temperature and inner-wall temperature, outer-surface temperature measurement, and detection of abnormal temperatures. In the central cloud structure of the original platform, all these tasks run on the temperature-measuring device, making the device heavily burdened. With 5G and fog computing layer, the functions that are relatively simple and closely related to the temperature measurement instruments, such as the initial position and angle optimization of temperature measurement, dual-phase synchronous control of horizontal motion and running rotation, and identification of cracking furnace tube outer-surface temperature and inner-wall temperature, are still retained on the temperature-measuring device, while more complex functions, such as overlapping tube identification, outer-surface temperature measurement, and abnormal temperature detection, are moved to the fog computing layer. The peep door status data is mainly acquired using the HD camera integrated in the intelligent temperature-measuring device in the format of video. The base station server receives the video signal and identifies the status of the peep door, which is combined with the intelligent peep door control signal to achieve precise control of the peep door.

Fog computing layer: It mainly includes 5G base station, base station server, and other network devices, forming a mini-data center, which is responsible for two main tasks. One is to further process the data transmitted by the intelligent temperature-measuring device, such as the overlapping tube identification, outer-surface temperature measurement, abnormal temperature detection, and transfer of the effective data to the cloud computing layer to reduce the amount of data uploaded to the cloud computing layer. The second is that the received video data is used to discriminate the peep door status using deep learning, migration learning, and other methods for the synchronized control of the intelligent peep door with the intelligent temperature-measuring device.

Cloud computing layer: As the central cloud, it runs the slagging diagnosis and prediction system of the ethylene cracking furnace tube and other systems of the enterprise. It receives temperature measurement data from the fog computing layer, combines the data from the data collection system located in the same cloud, and includes cracking furnace tube outlet temperature, crossover section pressure, and venturi pressure so as to achieve real-time accurate diagnosis of the slagging degree of the ethylene cracking furnace tube and accurate prediction of slagging trends. Meanwhile, the cloud computing layer is responsible for the training of intelligent models in the monitoring platform, such as the peep door status identification model and the overlapping tube identification model.

2) Edge-fog-cloud collaboration mechanism

The divide-and-conquer and north-south collaboration methods were adopted. The edge computing layer is the site work node, which consists of edge devices such as an intelligent temperature-measuring device and an intelligent peep door control device. It is responsible for transferring the collected outer-surface temperature data of the cracking furnace tube, video data monitoring of the peep door and edge device working-state data northward through 5G to the fog computing layer, and receiving the operation commands and trained intelligent models from the fog computing layer. The fog computing layer is an intermediate node consisting of the 5G base station, base station server, and other network devices. It further cleans and processes the data in the south direction and exchanges data and control signals with the edge computing layer. The north

direction exchanges data with the cloud computing layer and provides data support for the cloud computing layer. The cloud computing layer obtains valuable data from the fog computing layer for mass storage. On the one hand, intelligent models are trained and the automatic intelligent model update of the relevant edge devices is conducted to the fog computing layer server or through the fog computing layer. On the other hand, the data from other systems in the central cloud are combined to perform large data analysis, diagnose and predict the slagging of the cracking furnace tube, and provide decision support for production. The three layers of the edge-fog-cloud operate efficiently in a complementary manner through data collaboration, intelligence collaboration, and control collaboration.

The proposed edge-fog-cloud collaboration mechanism uses knowledge migration, embedded machine/deep learning, and other methods and techniques to optimize data collection, cleaning, transmission, storage, and application. The purpose is to achieve the collaboration of global optimization based on cloud computing and local optimization based on fog/edge computing through data collaboration, intelligence collaboration, and control collaboration. The working process of the next-generation platform involves three levels: data flow, control flow, and business flow. The whole platform's edge-fog-cloud collaborative capability and content include data collaboration, intelligence collaboration, and control collaboration, as shown in Figure 10.

Data collaboration: It consists of two data flows of tube temperature and peep door status. First, the intelligent temperature-measuring device in the edge computing layer initially processes and analyzes the collected data about the cracking furnace tube according to the rules or data model, and uploads the processing results to the fog computing layer through the 5G network. The fog computing layer further processes the received data and uploads it to the cloud computing terminal via a dedicated high-speed wired network. The cloud continuously receives data from the edge nodes and carries out a large data statistical analysis based on the massive operational status data (e.g., abnormal status data) to diagnose and predict the slagging degree of the cracking furnace tube. Second, the intelligent temperature-measuring device in the edge computing layer captures the video data of peep door status through the integrated camera and then uploads it to the fog computing layer through the 5G network. The fog computing layer uses a deep learning model to process the video to identify the state of the peep door, and uploads the key video to the cloud computing layer via a dedicated high-speed network for permanent storage. The data collaboration of edge, fog, and cloud supports the controlled and orderly flow of data between edge, fog, and cloud, forming a complete data flow path for efficient and low-cost data lifecycle management and value mining.

Intelligence collaboration: The temperature identification intelligent models are embedded in the intelligent temperature-measuring device for edge devices, while the fog computing layer integrates intelligent models for overlapping tube identification, abnormal temperature detection, and video identification. The operating environment of the cracking furnace tube is complex and variable. These models need to learn continuously to improve the self-adaptability of the temperature-measuring device and fog computing layer server, but learning training is a computationally intensive and time-consuming process. Therefore, the training task can only be placed in the cloud computing layer. The edge computing layer and the fog computing layer provide data input for the training of the model, and are responsible for the execution of edge inference. Considering the limited resource constraints of edge nodes, deploying AI chips or modules enables intelligence collaboration more efficiently. The cloud computing layer performs large data analysis by combining auxiliary data provided by other systems, continuously optimizes the model training,

and updates the trained model to the fog computing layer server or to the intelligent temperature-measuring device via the fog computing layer. Through intelligence collaboration, the self-directed learning of the fog computing server and the intelligent temperature-measuring device can be achieved.

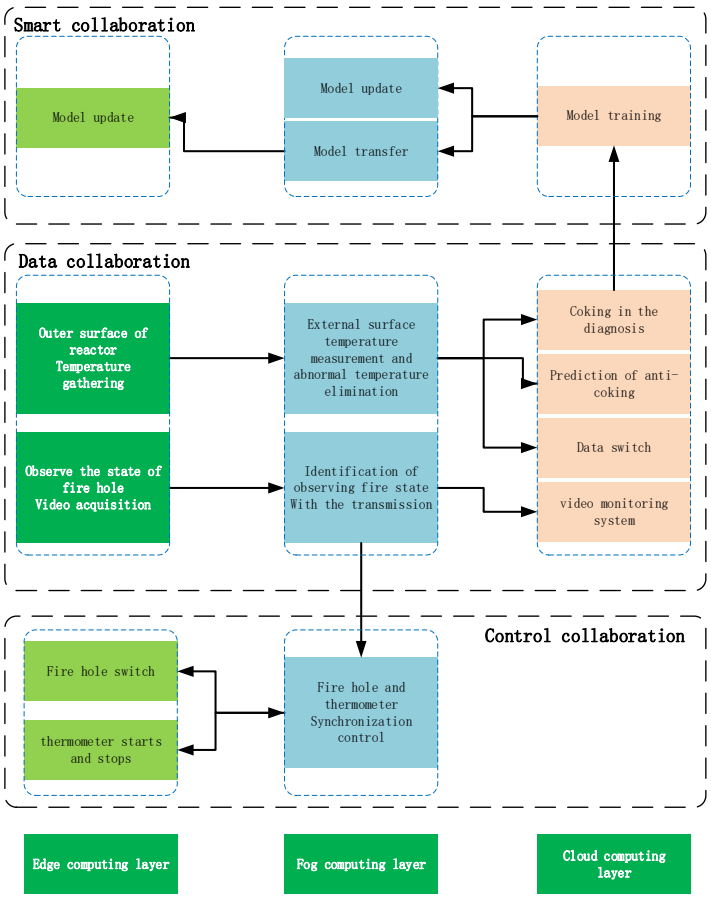

Figure 10. Edge-fog-cloud collaboration mechanism.

Control collaboration: The peep door must be opened and closed automatically to achieve full automation of the temperature measurement process. As the temperature-measuring device measures the temperature of the cracking furnace tube through the peephole, the opening angle of the peep door is strict during the temperature measurement. The whole control process is divided into seven steps:

Step 1: The fog computing layer server sends an open command to the intelligent peep door gearing according to a predefined policy.

Step 2: The fog computing layer server sends a video capture command to the temperature-measuring device.

Step 3: The fog computing layer server receives video signals from the edge computing layer and identifies the intelligent peep door status (e.g., whether it is open or closed).

Step 4: If the peep door has been opened at a sufficient angle, the temperature-measuring device is started for temperature measurement.

Step 5: When the temperature measurement is completed, a completion signal is sent to the fog computing layer server.

Step 6: The fog computing layer server sends a close command to the intelligent peep door gearing.
Step 7: Steps 2 and 3 are executed, if the peep door is closed; then the task is completed.

4. Applications of mixed deep learning algorithms

4.1. Identification of peep door status based on time-domain multiscale long short-term memory networks

4.1.1. Problem description

The identification of peep door status via the peep door surveillance video involves complex timing information. In the basic multilayer long short-term memory (LSTM) modeling sequential characteristic, the deep LSTM networks take the output of the previous layer of LSTM networks as the input at this moment. Not only do the deep LSTM networks lose the original video information, but also the training and information transfer of the networks may encounter bottlenecks. A time-domain multiscale space–time fusion model based on the multiscale feature in image processing was proposed to solve this problem, as shown in Figure 11. As observed, the video was sampled at different intervals, and the space–time fusion features of the video frame were used as the input of the network to obtain the time-domain features of the video content at different sampling intervals. The first-layer LSTM extracted 16 video frames, that is, video frame sequences $\{v_1, v_2, \ldots, v_{16}\}$ as the input. The second-layer LSTM halved the input of the first layer, that is, eight video frames $\{v_1, v_2, \ldots, v_8\}$ as the input. The input of the third-layer LSTM was halved from the second-layer input, that is, four video frames $\{v_1, v_2, \ldots, v_4\}$ were extracted as input to the LSTM networks. The detail technical details and experimental results can be seen in [20].

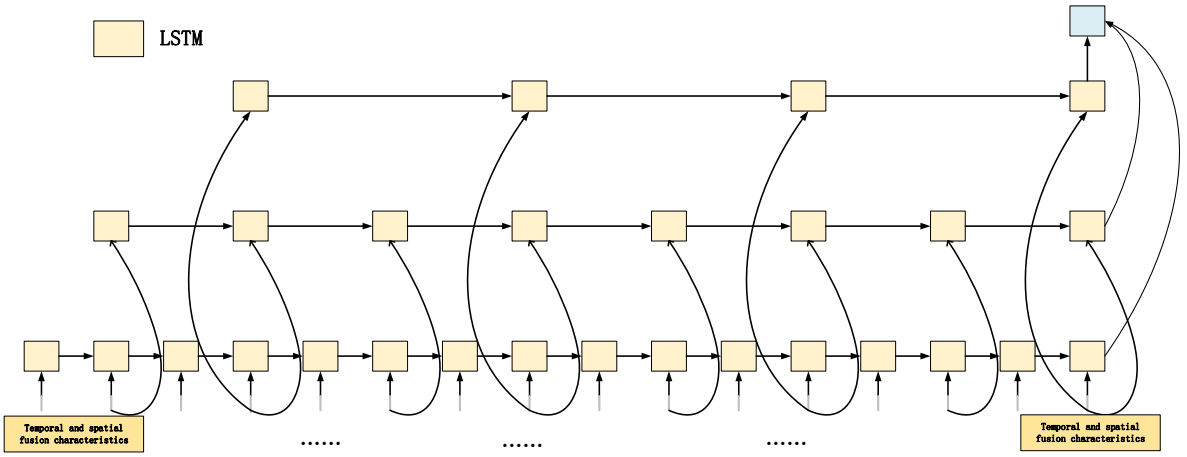

Figure 11. Time-domain multiscale space-time fusion model.

4.1.2. Experimental verification

1) Data set description

In terms of figure collection method, 150 pictures were taken by mobile phone. The size of the image after shooting is 2328 × 4656 pixels, and the format is JPG format. The default RGB color display standard is adopted, and three color channels are included. View of the shooting angle, for most images of fire door is not at the same level with the lens, lens is slightly higher than the view on

the location of the fire door view fire door, most image medium fire door in a look down at the point of view of another part of the pictures were taken in view of the fire door side, and there are four without fire door airtight cover images. Parts of peep door data set are shown in the Figure 12.

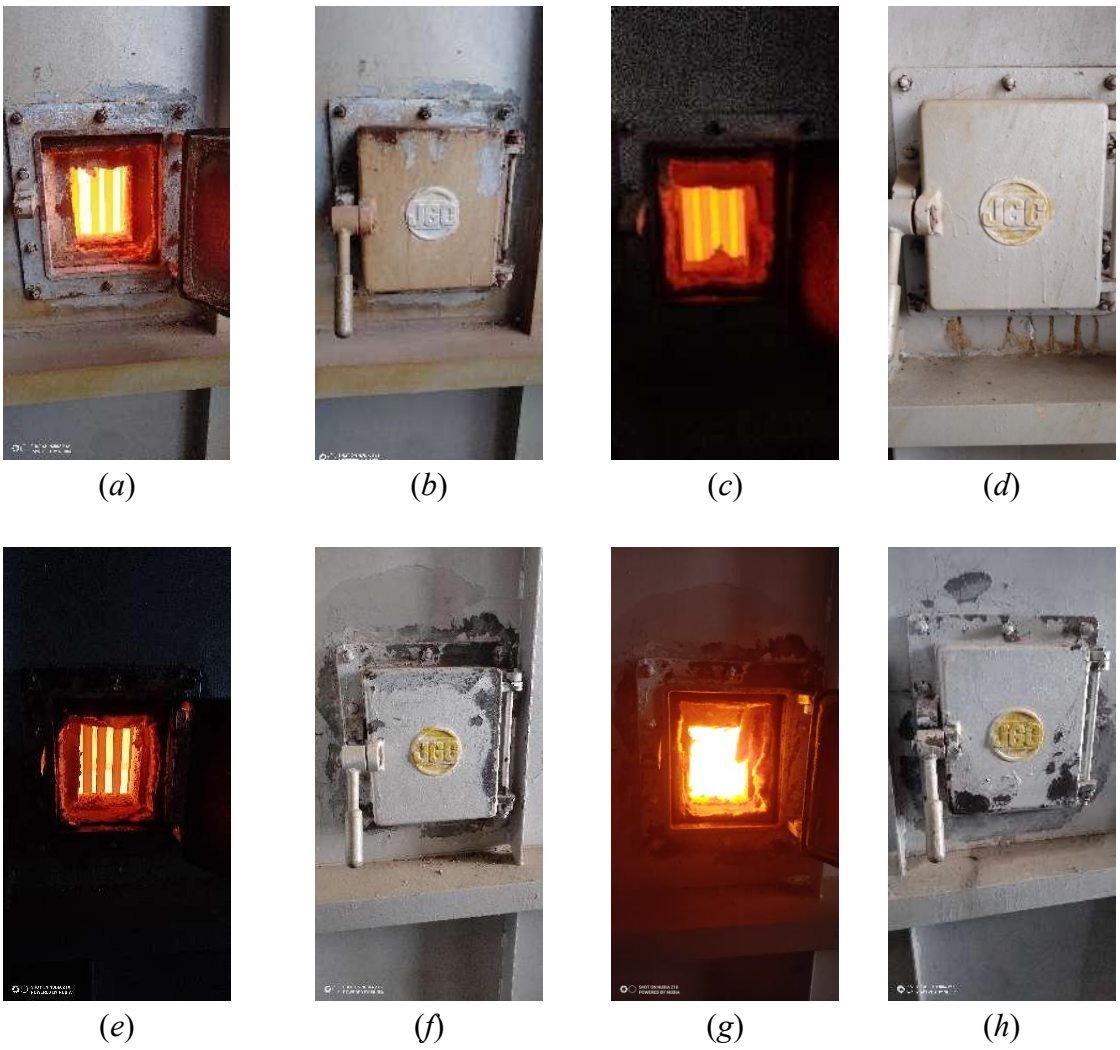

Figure 12. Parts of peep door data set.

2) Network structure and arameters

The keras framework in Tensorflow is used to construct the entire model structure. The structure of the convolutional neural network and parameters are shown in Table 1.

3) Model performance test

Figure 13 shows the accuracy and loss values of the training set and verification set respectively in the training process. A total of 10 epochs have been performed, and excellent recognition rate has been achieved in the first training.

Densenet-121 network is used for transfer learning, the results are shown in Figure 14. Results on the training set and the validation set is shown in Figure 14. The recognition model requires multiple epochs of training until the accuracy rate meets the re quirements. It is glad to see that the accuracy on the training set already reaches 95% after the fifth epoch. The accuracy on the validation set reaches 100%. After training four epochs, the proposed model has a 100% recognition rate on the

test set.

Table 1. Network structure and parameters.

Layer (type)	Output Shape	Param
conv2d_input (InputLayer)	[(n, 200, 200, 3)]	0
conv2d (Conv2D)	(n, 198, 198, 16)	448
max_pooling2d (MaxPooling2D)	(n, 99, 99, 16)	0
conv2d_1 (Conv2D)	(n, 97, 97, 32)	4640
max_pooling2d_1 (MaxPooling2)	(n, 48, 48, 32)	0
conv2d_2 (Conv2D)	(n, 46, 46, 64)	18,496
max_pooling2d_2 (MaxPooling2)	(n, 23, 23, 64)	0
flatten (Flatten)	(n, 33856)	0
dense (Dense)	(n, 512)	17,334,784
dense_1 (Dense)	(n, 1)	513

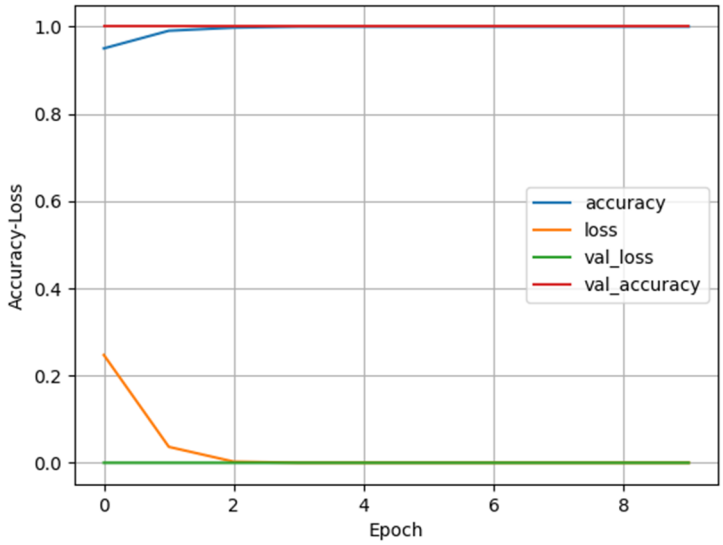

Figure 13. Model performance test.

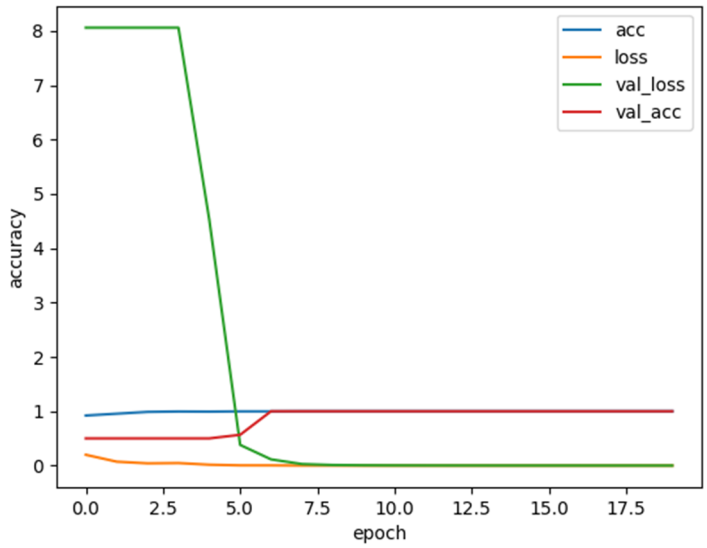

Figure 14. Densenet experiment results.

4.2. Overlapping tube identification algorithm based on embedded DCNN porting in the temperature-measuring device

4.2.1. Problem description

The overlapping tubes in the cracking furnace meant that the tubes were caused to block each other and the blocked tubes were only partially visible through the peephole during the production process due to the tube shift. Therefore, the intelligent temperature-measuring device required an efficient and accurate overlapping tube identification method during the measurement process to correctly distinguish the measured outer-surface temperature. Empirically, the intelligent temperature-measuring device could be used for overlapping tube identification using the point-counting method and the adjacent point distance jump method, but the identification rate was low with a tendency for misjudgment situations and the most serious overlapping tubes were completely blocked, as shown in Figure 15, which led to the serious consequence of mismeasurement of the tube outer-surface temperature.

Based on the difference between normal and overlapping tubes in the measured temperature and distance 2D data and the advantage of DCNN in identifying 2D image features, DCNN was transplanted to the embedded chip of the edge device (intelligent temperature-measuring device), and the compressed DCNN was used on the edge side to identify overlapping tubes and normal tubes with high accuracy.

The DCNN for determining overlapping tubes is shown in Figure 16. It consisted of one input layer, three convolutional layers, two pooling layers, one fully connected layer, and one output layer. The input layer was used to input the 2D data features of normal and overlapping tubes, and the output layer was used to output the probability that the 2D data features belonged to normal and overlapping tubes.

During feature extraction of tube distance data in the 2D map, the temperature data of tubes and furnace walls in the 2D map were removed first, and then the distance data of furnace walls in the 2D

map were removed. Further, the invalid threshold data of tube distance data having low feature correlation with overlapping tubes were removed so that the feature maps of overlapping and nonoverlapping tubes were extracted to form the dataset for DCNN network model training. After extracting the tube features, the DCNN overlapping tube identification model was trained and validated in cloud.

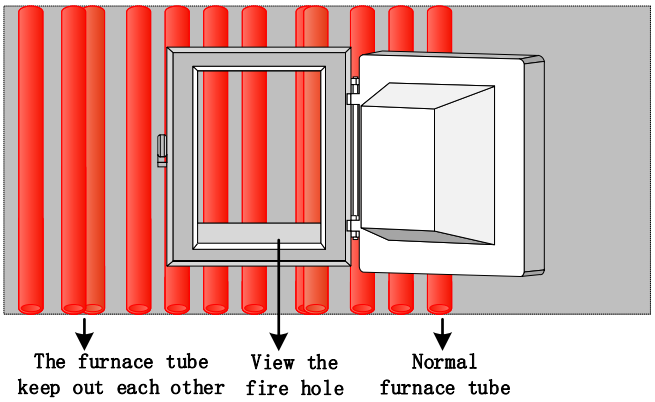

Figure 15. Schematic of overlapping tubes.

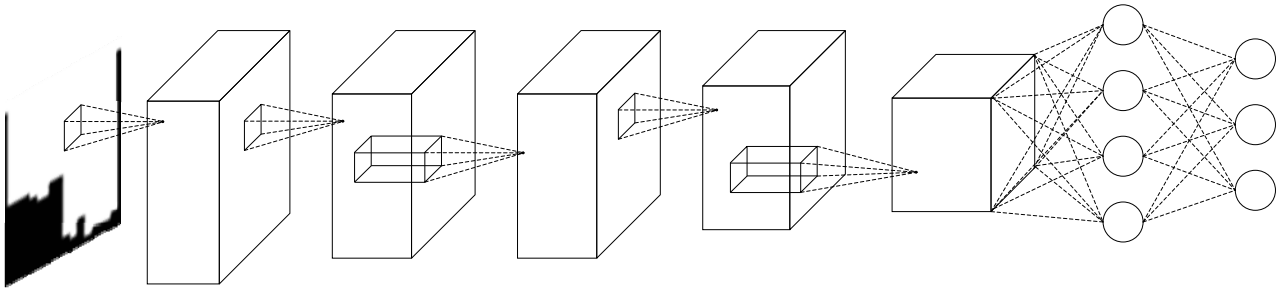

Figure 16. DCNN structure for determining overlapping and nonoverlapping tubes.

For realizing the overlapping tube identification function of the intelligent temperature-measuring device, the proposed steps to implement the DCNN overlapping tube identification inside the intelligent temperature-measuring device with an embedded processor as the core were as follows:

Step 1: DCNN training weights were compressed, transformed, and ported. In the cloud server, the DCNN network model for identifying normal and overlapping tubes was first trained, and then the trained network model was compressed using the NCS-based method. Further, the compressed DCNN node weights were transformed into data types that could be stored and computed inside the ARM Cortex-M7 embedded processor. Finally, the transformed weights were embedded in the embedded processor.

The ARM Cortex-M7 embedded processor only received 8-bit fixed-point numbers; therefore, the DCNN node weights data type needed to be compressed and transformed. The compression conversion process to be adopted was as follows: a generalized fixed-point number was represented as [QI: QF], where QI and QF corresponded to the integer and fractional parts, respectively. The fixed-point number usually included a sign bit to indicate the positive or negative of the number. The

relationship between the integer length (IL), fractional length (FL), and length of sign bits of the fixed-point number, and bit-width (B) of the bit number of fixed-point number was as follows:

$$B = FL + IL + 1 \tag{1}$$

When converting floating-point numbers into fixed-point numbers, a specific rule was proposed to automatically determine the number of integer bits required. Specifically, enough bits were selected to avoid saturation. Therefore, for a given set of numbers S, the required length of the integer part was as follows:

$$IL_S = \lceil \log_2 (\max_S x + 1) \rceil \tag{2}$$

where $\lceil x \rceil$ denotes the rounding up for x.

For conversion into fixed-point numbers with specified bit-width N, the length of the integer part IL was determined by:

$$IL = \begin{cases} IL_S & , IL_S < N - 1 \\ N - 1 & , IL_S \geq N - 1 \end{cases} \tag{3}$$

The length of the fractional part could be calculated by:

$$FL = N - IL - 1 \tag{4}$$

The minimum positive number of the fixed-point number representation was defined as ε, which was the representation precision of the fixed-point number as ε. The formula was as follows:

$$\varepsilon = 2^{-FL} \tag{5}$$

Therefore, a given floating-point number could be converted into an approximation of the specified bit-width according to the following equation, which facilitated the subsequent fixed-point conversion of the value:

$$fixed(x) = \begin{cases} \lfloor x \rfloor & , \lfloor x \rfloor \leq x \leq \lfloor x \rfloor + \frac{\varepsilon}{2} \\ \lfloor x \rfloor + \varepsilon & , \lfloor x \rfloor + \frac{\varepsilon}{2} < x \leq \lfloor x \rfloor + \varepsilon \end{cases} \tag{6}$$

where $\lfloor x \rfloor$ is defined as a value less than or equal to x and is the largest integer multiple with respect to ε.

For a fixed-point number given bit-width, the numerical approximation took the range:

$$\begin{cases} -2^{IL-1} & , x \leq -2^{I-1} \\ 2^{I-1} - 2^{-FL} & , x \geq 2^{IL-1} - 2^{-FL} \\ fixed(x) & , otherwise \end{cases} \tag{7}$$

After the approximation of the original values, the fixed point of approximate value was implemented, and the fixed-point formula was as follows:

$$value = (-1)^s \cdot 2^{-FL} \cdot \sum_{i=0}^{B-2} 2^i \cdot x^i \tag{8}$$

where x represents the binary complement form of the approximation.

Once the fixed point was complete, the fixed-point weights were finally ported to the embedded processor.

Step 2: DCNN reconstruction. The implementation of DCNN reconstruction within the embedded processor applied the ported compressed fixed-point weights for network computation and relied on CMSIS-NN, an optimization software kernel proposed by ARM specifically for deploying neural networks on Cortex-M CPUs. The CMSIS-NN library contained two parts: NNFunction and NNSupportFunctions. The NNFunction contained functions that implemented common neural network layer types, such as convolution, full connectivity, pooling, and activation functions, which were used by the application code to implement neural network inference applications. The NNSupportFunctions included different utility functions, such as data conversion and activation menu functions, which could be used by the application code to construct more complex neural network modules.

Step 3: The raw data collected were converted. The original one-dimensional data collected by the temperature-measuring device were converted into two-dimensional feature data, which were fed into the embedded processor reconstructed DCNN network and combined with the compressed and transformed weights to realize the function of DCNN to identify normal and overlapping tubes. The 2D data were obtained by dimensionally transforming the one-dimensional tube feature data obtained from the temperature-measuring device, which was used as the input to the embedded DCNN network.

4.2.2. Experimental verification

The parameter settings of the CNN network are shown in Table 3, and the sample composition is shown in Table 4.

Table 3. Network structure and parameters.

Parameter	Value	Parameter	Value
test_iter	40	gamma	0.0001
base_lr	0.001	power	0.75
momentum	0.9	display	500
weight_decay	0.0005	max_iter	10,000

Table 4. Structural composition of experimental data.

Sample	Normal	Overlapped	Total
Training	1,456	608	2064
Test	1,028	412	1440

1) Model Validity Performance Test

The main steps and model performance test are as follows, and the detail technical details and experimental results can be see in [22].

Step 1: The furnace wall distance was removed from the original collection distance data, as shown in Figure 17 below:

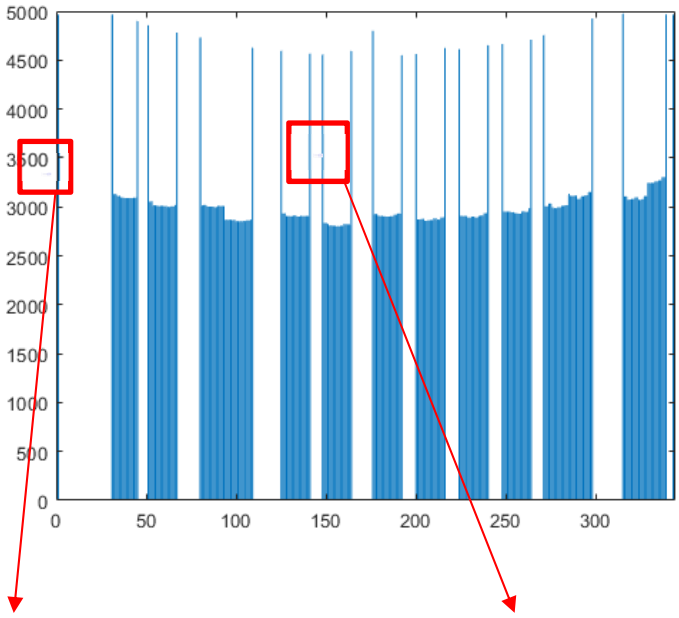

Figure 17. Data eliminate.

Step 2: Extract the features of each normal tube and overlap tube, as shown in Figure 18:

Figure 18. The features of each normal tube and overlap tube.

Step 3: The training set is used to train the CNN network, and the validation set is used to judge the effect of the training model and optimize network parameters during the training process, the recognition results are shown in the Figure 19, the results show the output accuracy is 100%.

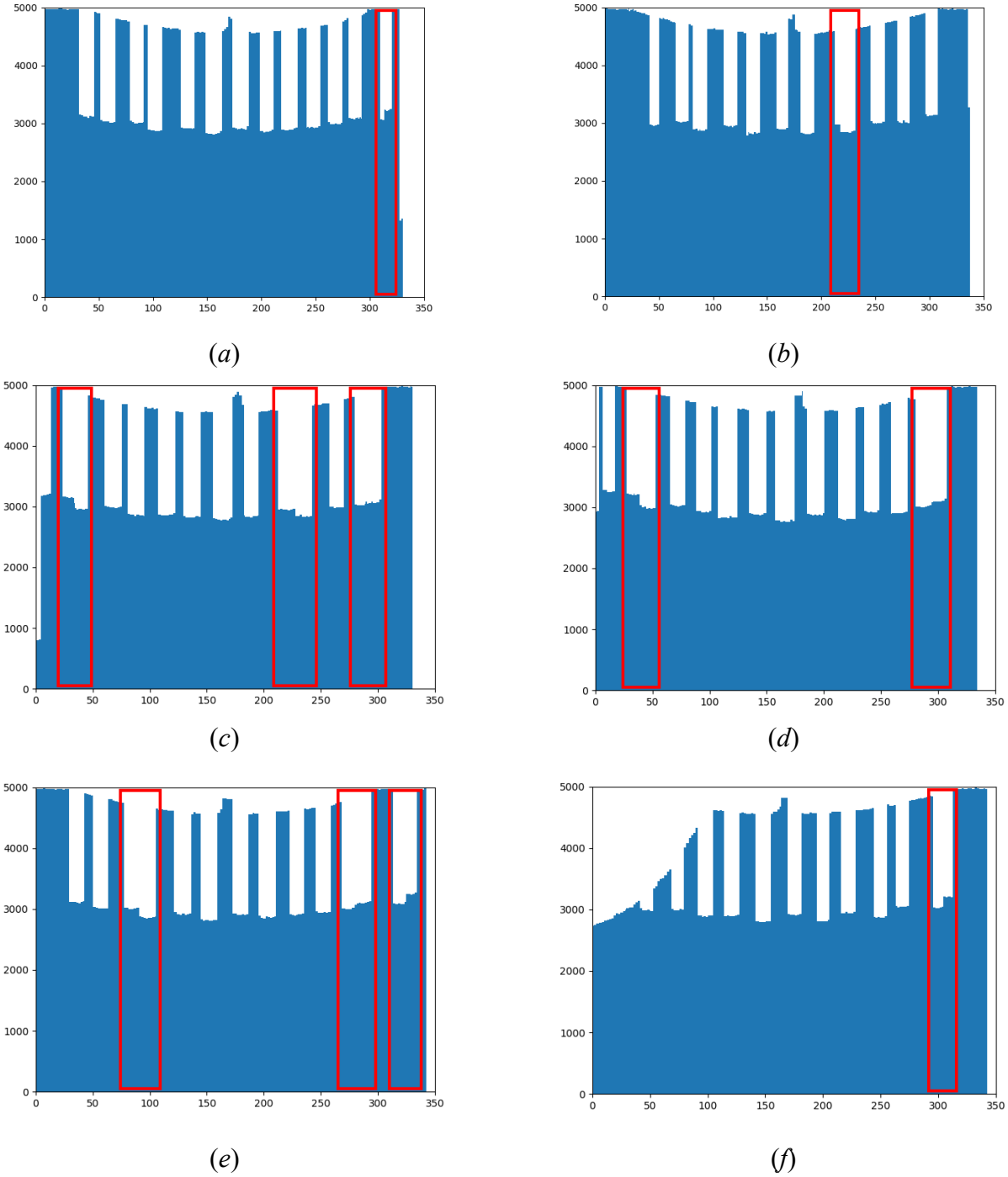

Figure 19. Model validity performance test.

2) Model performance comparative analysis

In the experiment, six different learning strategies such as Fixed, STEP, EXP, INV, Poly and SigmoID were used to train the model. The change curve of model accuracy during training is shown in Figure 18. It can be seen from Figure 20 that the final accuracy of the overlapping furnace tube identification model trained by other methods except step and EXP is 99.85%.

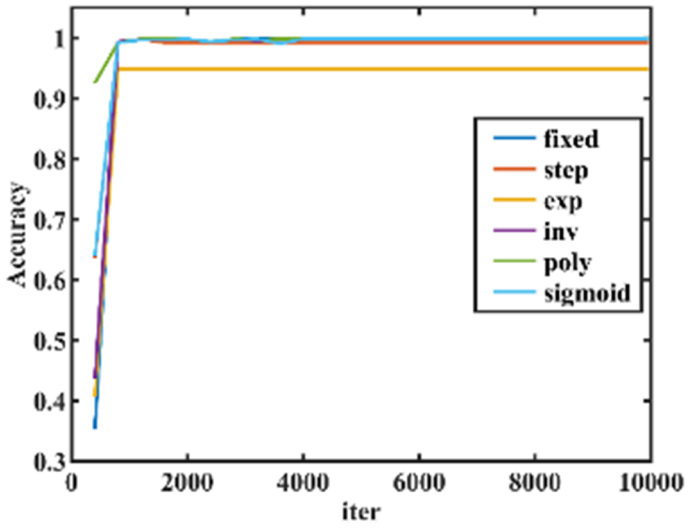

Figure 18. Comparison chart of different learning strategies.

4.3. Edge computing resource scheduling based on deep reinforcement learning

4.3.1. Problem description

The intelligent temperature-measuring device was a typical mobile edge terminal device, which ran monitoring tasks in a remote data center through a high-speed and highly reliable wireless interface. The tasks were transmitted through the wireless access network and then through the core network to the data center. Nevertheless, this model had an inherent drawback due to the long-distance propagation from the end device to the data center. The message delivery needed to go through the wireless access network, backhaul network, where the network routing and management operations might add additional time delay overhead. For this reason, the industry has proposed mobile edge computing (MEC). MEC refers to the deployment of computing and storage resources at the mobile network edge to provide IT service environment and computing power for mobile networks, thus providing users with ultra-low time delay and high-bandwidth network service solutions, while enhancing the privacy and security of mobile applications. Although a certain amount of computing resource is placed at the access network edge, MEC can reduce the application time delay through computational offloading. However, with limited communication and computing resources, designing a reasonable offloading strategy and resource allocation scheme is still an issue to be explored.

For the limited computing resource, communication resource, and local computing resource, an effective computation offloading and resource allocation strategy was designed based on the deep reinforcement learning method in combination with 5G communication technology so that all tasks could be executed with minimum total time delay.

The objective of uninstall decisions of edge devices, such as multiple intelligent temperature-measuring devices in the system and the allocation of network and computing resources, was to minimize the total time delay of all tasks, and the problem was represented as follows:

$$\min_{c_n, t_n^{exe}, t_n^{off}} \sum_{n=1}^{N} c_n T_n^l + (1 - c_n) T_n^o$$
$$s.t. \qquad c_n \in \{0, 1\} \tag{9}$$
$$t_n^{exe} \geq t_n^{off} + T_n^t$$

where *Cn* represents the uninstall decision variable. As the task was nonseparable, the uninstall decision variable for edge device n is an integral 0, 1 variable. The second constraint indicated that the task needed to be uploaded to the MEC server first before it could be executed.

To solve this problem, we needed to determine three decision variables, which were the uninstall decision variable, the upload data time of the uninstall task, and the execution time. As the number of edge devices increased, the solution space size of the problem increased rapidly. Meanwhile, because the three decision variables were integer variables, the problem was not a convex optimization problem, but an NP-hard problem. Hence, the problem was solved using deep reinforcement learning methods.

It is first necessary to translate the problem into a representation of the basic elements of reinforcement learning to find the optimal strategy using the deep reinforcement learning approach. Second, the parameters of the deep learning network structure needed to be determined because deep learning was used as a reinforcement learning agent. Figure 19 shows the MEC resource scheduling model based on deep reinforcement learning.

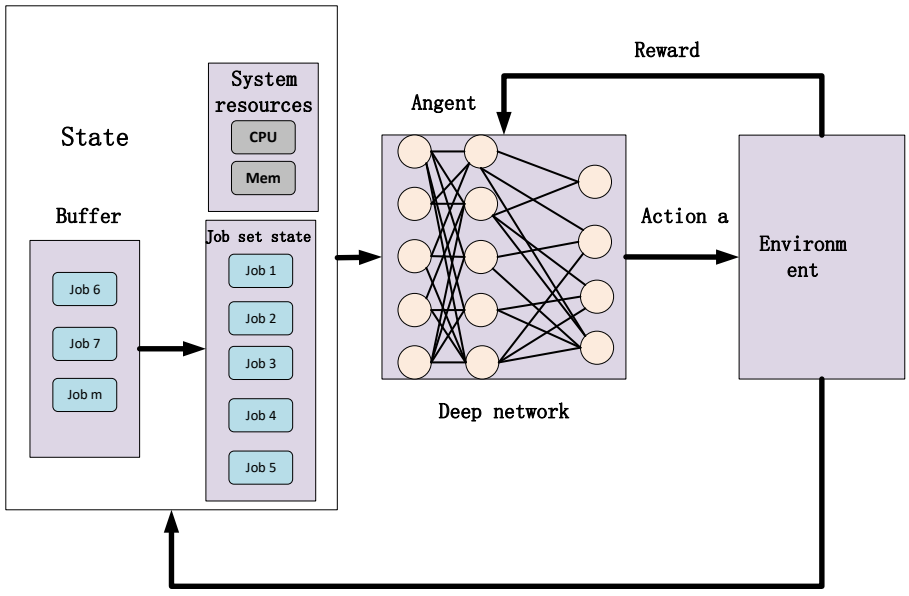

Figure 19. MEC resource scheduling model based on deep reinforcement learning.

4.3.2. Related concept of deep reinforcement learning

Reinforcement learning comprised four components: state, action, reward, and agent. The agent in deep reinforcement learning was a neural network, that is, the strategy was represented by a deep learning network. The state, action, and reward were designed as follows.

Status: In the MEC resource scheduling problem of this project, the status should include the network resource usage of the base station, the MEC server computing resource usage, and the tasks waiting for a decision in the mobile device. Figure 20 shows the network resources and computing resource occupancy from the current time slice to the next few time slices. The vertical direction represented the time slices to be allocated, and each small square represented a time slice resource. The horizontal direction represented the resource category, that is, computing resource or network resource. When the edge device had a task to perform, it first sent a request to the base station. The base station stored the corresponding task information, that is, network resource consumption, computing resource consumption, and channel status, in the backlog. When the job slot queue was empty, the base station scheduled the task from the backlog to the job slot and waited for the base station's decision on the task scheduling. In the job slot queue, tasks were represented as the number of time slices of network resources to be consumed and the number of computing resource time slices.

Action: It used deep learning as an agent, requiring a fixed input and output form. Therefore, the action space could not change as the number of tasks in the state changed. The action space should contain all uninstall possibilities. As the tasks waiting to be scheduled could choose some tasks uninstalled to the base station and others were executed on the local side, the agent could choose any part of the tasks waiting to be scheduled as an execute decision uninstalled to a base station and other tasks were executed on the local device. The relationship between the size of action space and the number n of tasks to be scheduled was 2^n, that is, any task could be scheduled to the base station and also be executed on the local device. As the number of tasks to be scheduled increased, the action space increased drastically, which did not meet the requirement of fixed action space for the neural network output. Therefore, the following method was used to reduce the action space size.

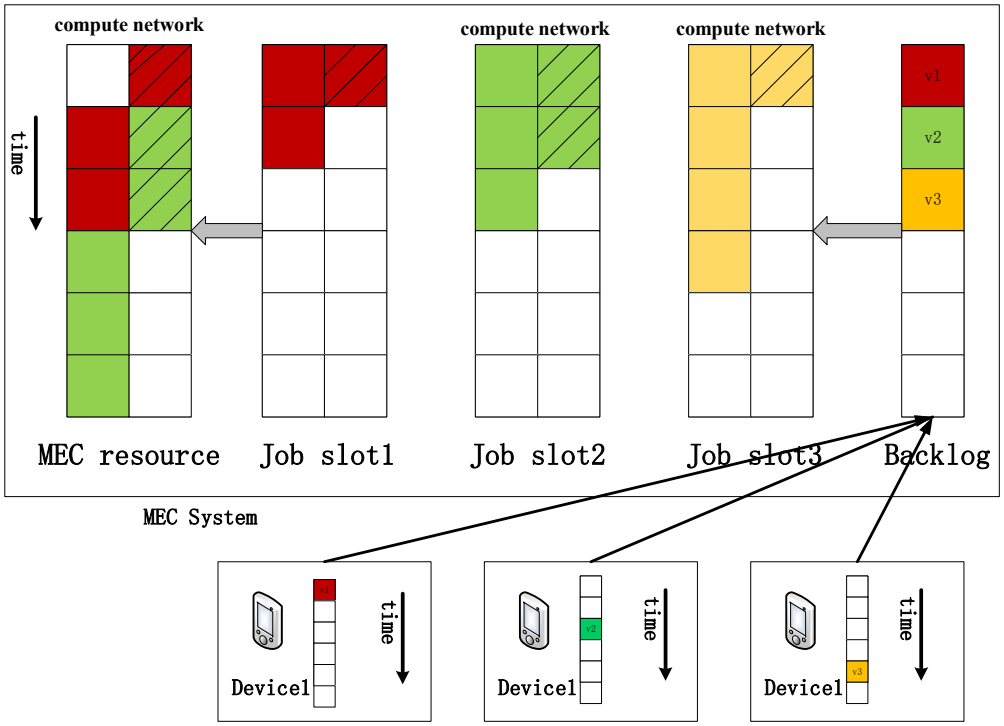

Figure 20. State representation.

In each time slice, the base station could execute more than one task in a row. In the state, the tasks to be scheduled included tasks in the job slot and backlog queue. It was assumed that the size of the job slot was k and the action space was $\{0, 1, 2, \cdots, 2k\}$, where $a = 0$ meant no task to be scheduled and it was an empty action. $a \in \{0, 1, 2, \cdots, k\}$ meant that the base station chose to uninstall the task on the ath job slot to the base station side. $a \in \{k+1, k+2, \cdots, 2k\}$ meant that the base station chose the task on the $a-k$th job slot to execute in the edge device.

Reward: Agents in reinforcement learning were designed to maximize the cumulative discounted rewards over time, that is, the value function:

$$R = \sum_{t=0}^{n} \gamma^n r_t \tag{10}$$

where γ is the discount factor, and r_t represents the reward at state t. The goal of this problem was to minimize the total time delay of all tasks. Specifically, the reward function was set as follows:

$$r_t = \sum_{j \in J} -1 \tag{11}$$

where j represents all the tasks in the state and the tasks performed by the local device. As reinforcement learning had a reward for each action selection, the reward was 0 when the action was a valid action defined in the action space, and the reward was the value of reward function in Eq (11) when the action was an invalid action defined in the action space. In other words, the evaluation of the agent uninstall policy in this time slice needed to wait until the invalid action was generated, at which point the reward of Eq (11) was given, while the valid action indicated that the task uninstall was not finished in this time slice and returned to 0. After a task was executed on the edge device or base station side, it no longer belonged to *J*. The discount factor was set to 1, so that the –1 accumulation of all time slices occupied by a task from the time the uninstall request was sent until it was executed represented a negative time delay in execution. The optimization of deep learning parameters used the gradient descent method, that is, minimized the loss function. While reinforcement learning maximized the long-term reward value, in deep reinforcement learning, the long-term reward was the loss function. Therefore, the reward of the aforementioned design was a negative time delay sum, and maximizing the negative time delay sum meant minimizing the total time delay.

4.3.3. Experimental verification

The train model parameter settings of the DQN are shown in Table 5, and the network parameters is shown in Table 6.

1) Convergence verification

Compared with classical heuristic short-job priority SJF algorithm, Teris* algorithm and strategy gradient algorithm DeepRM, the results of the experiment are shown in Figure 21. Compared with DeepRM, DQN algorithm shows faster convergence and more stable curve. Compared with DeepRM algorithm, the average completion time of the final convergent job is reduced by 5.2%. During the whole training process, the DQN and DeepRM curves were unstable

and oscillating in the first 100 iterations, and the average completion time was longer than that of the heuristic SJF algorithm and Teris* algorithm. After 200 rounds of training, the curve gradually tends to be stable, and the completion time is significantly lower than SJF algorithm and Teris* algorithm, and finally tends to converge. And the detail technical details and experimental results can be seen in [28–30].

Table 5. DQN train model parameters.

Parameter	Value	Parameter	Value
Train time	1000	Greedy factor ε initial value	0.5
Learning rate	0.001	Greedy factor ε max value	0.9
Discount factor	0.95	Ɛ amplification	0.001
Target network update interval	100	Round number	20
Experience pool size	30000	Mini-batch	32

Table 6. Network parameters.

Net layer	Convolution layer	Maximum pooling layer	Full connection layer
Input size	180 * 20	178 * 18	89 * 9
Convolution kernel size	2 × 2	2 × 2	--
Step size	(1,1)	(2,2)	--
Number fo convolution kernel	8	--	--
Activation function	ReLU	--	--
Output size	178*18	89*9	21

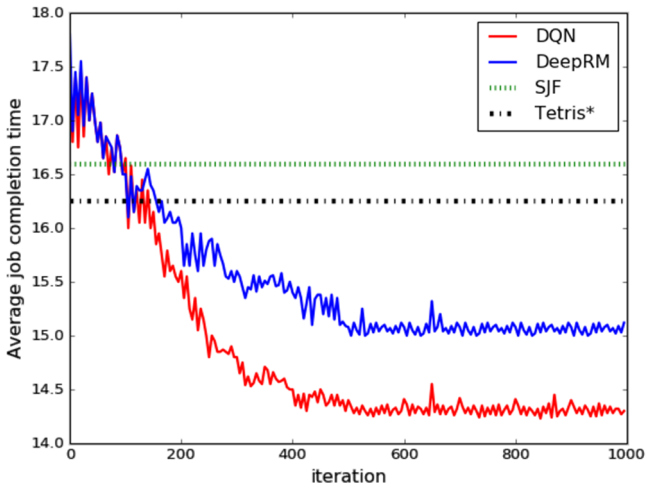

Figure 21. Average job completion time.

2) Validity verification

Figure 22 shows the change trend of the average operation sabotage of the four comparison algorithms under different loads. As shown in the figure, under the condition of low load, there is little difference in the change of different algorithms. When the load reaches or exceeds 90%, it can be clearly observed that the average operation sabotage change rate of DeepRM and DQN algorithms

is small. The results were significantly lower than those of the heuristic algorithms SJF and Tetris*. The results also shows that when the load reaches 130% and the training times reaches 200 rounds, DQN and DeepRM algorithms begin to converge, and the convergence result is smaller than SJF and Tetris*. At the same time, DQN converges faster than DeepRM and achieves smaller average operation slowdowns.

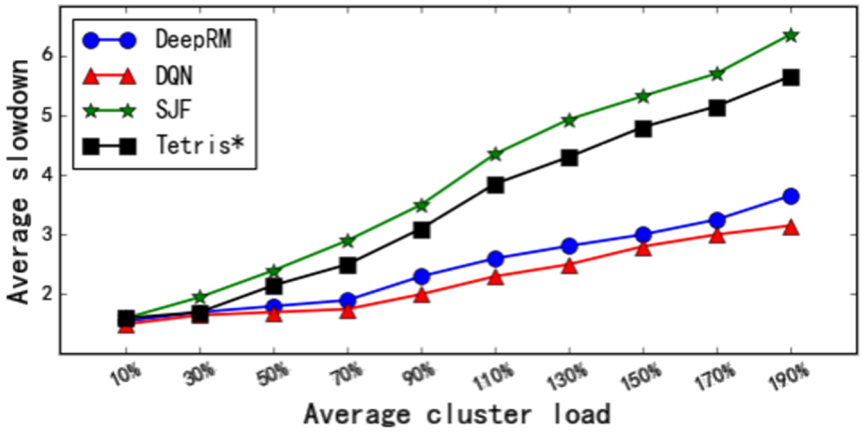

Figure 22. Job slowdown under different loads.

4.4. Comparison of the 5G fusion-based next-generation intelligent health-monitoring platform for ethylene cracking furnace tubes and the previous platform

Compared with the previous platform, the 5G-based next-generation intelligent health-monitoring platform for ethylene cracking furnace tubes had a clear advantage (Table 7). The application site of this platform in a large petrochemical company is shown in Figure 23.

Figure 23. Application of intelligent temperature-measuring device and software in petrochemical enterprises.

Table 7. Next-generation platform versus the previous platform.

Function or technology	Next-generation platform	Previous platform
Network transmission technology	5G-based	LoRa-based
Temperature measurement method	Remote automated control in the workshop	Manual control at the cracking furnace site
Peep hole operational condition monitoring	Real-time video remote monitoring	Manual on-site visual inspection
Peep hole initial operation parameter setting	Fully adaptive	Manual measurement
Self-learning of temperature-measuring device	Strong	Weak
Peep door	Intelligent type, automatic open and close	Mechanical type, manual open and close
Identification of overlapping tubes	≥ 99.99%	About 80%
Charging of temperature-measuring device	Automatic	Manual
Deep network model	Compressed	Not compressed
Platform structure	Edge-fog-cloud three-layer structure	Central cloud structure
Computing resource scheduling	Based on deep reinforcement learning, resource utilization is higher	Based on reinforcement learning, resource utilization needs to be improved
Temperature measurement time per cycle	≤ 7 min	~10 min

5. Conclusions

Considering the technology demand from ethylene production industry and market, a next-generation intelligent health-monitoring platform was built based on 5G + mixed computing + deep learning for ethylene cracking furnace tubes deriving from the previously developed platform and its successful application. The key common problems in the platform, such as 5G-based intelligent temperature-measuring device, 5G-based intelligent peep door gearing, 5G-based edge-fog-cloud collaboration mechanism, and mixed deep learning application, were also examined. The aim was to improve the overall performance of the platform, enhance the automation and intelligence level of the platform, further promote the quality and efficiency of the enterprise, better protect the safe operation of the cracking furnace device, and also promote the industry-scientific and technological progress, transformation, and upgrading through the application of the platform.

Acknowledgments

This study was supported by the National Natural Science Foundation of China (61772145, 61672174), the Guangdong Basic and Applied Basic Research Foundation (2021A1515012252,

2020A1515010727, 2022A1515012022), the Key Field Special Project of the Department of Education of Guangdong Province (2020ZDZX3053), the Key Realm R&D Program of Guangdong Province (2021B0707010003), and the Maoming Science and Technology Project (210429094551175, mmkj2020008, and mmkj2020033), 2022 Guangdong Province Science and Technology Innovation Strategy Special Project (pdjh2022b0349).

Conflict of interest

The authors declare there is no conflict of interest.

References

1. F. Qian, W. Du, W. Zhong, Y. Tang, Problems and challenges of smart optimization manufacturing in petrochemical industries (in Chinese), *Acta Autom. Sini.*, **43** (2017), 893–901. https://doi.org/10.16383/j.aas.2017.c170129
2. T. Chai, Q. Liu, J. Ding, Perspectives on industrial-internet-driven intelligent optimized manufacturing mode for process industries (in Chinese), *Sci. Sin. Tech.*, **52** (2022), 14–25. https://doi.org/c10.1360/SST-2021-0405
3. N. Ma, X. Yao, K. Wang, Current status and prospect of future internet-oriented wisdom manufacturing (in Chinese), *Sci. Sin. Tech.*, **52** (2022), 55–75. https://doi.org/10.1360/SST-2021-0232
4. Y. Shi, Q. Han, W. Shen, L, Wang, X. Wang, 5G Applications of intelligent manufacturing scenarios, *China Mech. Eng.*, **31** (2020), 227–236. https://doi.org/10.16157/j.issn.0258-7998.211944
5. Y. Shu, F. Zhu, An edge computing offloading mechanism for mobile peer sensing and network load weak balancing in 5G network, *J. Ambient Intell. Hum. Comput.*, **11** (2020), 503–510. https://doi.org/10.1007/s12652-018-0970-5
6. S. Wang, Measures for realizing long period efficient operation of cracking furnace, *Refin. Chem. Ind.*, **29** (2018), 30–32. https://doi.org/10.3969/j.issn.1671-4962.2018.01.010
7. H. Wang, *Ethylene Plant Technology and Operation*, China Petrochemical Press, 2009.
8. X. Sun, L. Shen, Research progress of coking mechanism and prevention measures for ethylene cracking furnace tubes, *Corros. Sci. Prot. Technol.*, **29** (2017), 575–580. https://doi.org/10.11903/1002. 6495.2017.034
9. Y. Jin, J. Li, W. Du , Z. Wang, F. Qian, Outlet temperature correlation and prediction of transfer line exchanger in an industrial steam ethylene cracking process, *Chin. J. Chem. Eng.*, **21** (2013), 388–394. https://doi.org/10.1016/S1004-9541(13)60472-8
10. H. Shi, B. Peng, X. Jiang, C. Su, J. Cao, P Li, A hybrid control approach for the cracking outlet temperature system of ethylene cracking furnace, *Soft Comput.*, **24** (2020), 12375–12390. https://doi.org/10.1007/s00500-020-04679-0
11. S. Fedorov, A. Krasnov, M. Prakhova, Algorithm for diagnostics of technical condition of the tube furnace coils, in *2020 International Multi-Conference on Industrial Engineering and Modern Technologies (FarEastCon)*, (2020), 1–6. https://doi.org/10.1109/FarEastCon50210.2020.9271548

12. S. Vangaever, P. Reyniers, S. Symoens, N. Ristic, M. Djokic, G. Marin, Pyrometer-based control of a steam cracking furnace, *Chem. Eng. Res. Des.*, **153** (2020), 380–390. https://doi.org/10.1016/j.cherd.2019.10.023
13. N. Gillani, T. Arslan, Intelligent sensing technologies for the diagnosis, monitoring and therapy of alzheimer's disease: a systematic review, *Sensors*, **21** (2021), 4249. https://doi.org/10.3390/s21124249
14. Y. Dai, H. Hu, M. Wang, J. Xu, S. Wang, Stretchable transistors and functional circuits for human-integrated electronics, *Nat. Electron.*, **4** (2021), 17–29. https://doi.org/10.1038/s41928-020-00513-5
15. G. Niu, S. Yu, Application of infrared on line temperature field detection system in ethylene pyrolyzer, *Autom. Petro-Chem. Ind.*, **56** (2020), 72–74.
16. D. Pinnock, P. Maropoulos, Review of industrial temperature measurement technologies and research priorities for the thermal characterisation of the factories of the future, *Proc. Inst. Mech. Eng., Part B: J. Eng. Manuf.*, **230** (2016), 793–806. https://doi.org/10.1177/0954405414567929
17. B. Rizkin, K. Popovich, R. Hartman, Artificial neural network control of thermoelectrically cooled microfluidics using computer vision based on IR thermography, *Comput. Chem. Eng.*, **121** (2019), 584–593. https://doi.org/0.1016/j.compchemeng. 2018.11.016
18. G. Mei, J. Zhang, S. Zhao, Z. Xie, Simple method for calculating the local effective emissivity of the blackbody cavity as a temperature sensor, *Infrared Phys. Technol.*, **85** (2017), 372–377. https://doi.org/10.1016/j.infrared.2017.07.019
19. C. Abram, B. Fond, F. Beyrau, Temperature measurement techniques for gas and liquid flows using thermographic phosphor tracer particles, *Prog. Energy Combust. Sci.*, **64** (2018), 93–156. https://doi.org/10.1016/j.pecs.2017.09.001
20. Q. Li, B. Zhang, D. Cui, The research of recognition of peep door open state of ethylene cracking furnace based on deep learning, *Math. Biosci. Eng.*, **19** (2022), 3472–3486. https://doi.org/10. 3934/mbe. 2022160
21. Z. Peng, J. He, Y. Tan, D. Cui, Q. Li, J. Qiu, Study of dual-phase drive synchronization method and temperature measurement algorithm for measuring external surface temperatures of ethylene cracking furnace tubes, *Appl. Petrochem. Res.*, **8** (2018), 163–172. https://doi.org/10.1007/s13203-018-0205-x
22. J. Zhao, Z. Peng, D. Cui, Q. Li, J. He, J. Qiu, A method for measuring tube metal temperature of ethylene cracking furnace tubes based on machine learning and neural network, *IEEE Access*, **7** (2019), 158643–158654. https://doi.org/10.1109/ACCESS.2019.2950419
23. J. Lee, K. Lee, A. Yoo, C. Moon, Design and implementation of edge-fog-cloud system through HD map generation from LiDAR data of autonomous vehicles, *Electronics*, **9** (2020), 2084. https://doi.org/10.3390/electronics9122084
24. K. Geihs, H. Baraki, D. Oliva, Performance analysis of edge-fog-cloud architectures in the Internet of things, in *2020 IEEE/ACM 13Th International Conference On Utility And Cloud Computing (UCC 2020)*, (2020), 374–379. https://doi.org/10.1109/UCC48980.2020.00059
25. A. Alharbi, M. Aldossary, Energy-efficient edge-fog-cloud architecture for IoT-based smart agriculture environment, *IEEE Access*, **9** (2021), 110480–110492. https://doi.org/10.1109/ACCESS. 2021.3101397

26. X. Wang, Y. Han, V. M. Leung, D. Niyato, X. Yan, X. Chen, Convergence of edge computing and deep learning: a comprehensive survey, *IEEE Commun. Surv. Tutorials*, **22** (2020), 869–904. https://doi.org/10.1109/COMST.2020.2970550
27. Y. Shi, J. Sun, D. Liu, L. Kou, B. Li, Q. Yang, et al., Cloud-based data offloading for multi-focus and multi-views image fusion in mobile applications, *Mobile Networks Appl.*, **26** (2021), 830–841. https://doi.org/10.1007/s11036-019-01326-3
28. D. Cui, Z. Peng, J. Xiong, A reinforcement learning-based mixed job scheduler scheme for grid or IaaS cloud, *IEEE Trans. Cloud Comput.*, **8** (2020), 1030–1039. https://doi.org/10.1109/TCC.2017.2773078
29. K. Li, Z. Peng, D. Cui, SLA-DQTS SLA constrained adaptive online task scheduling based on DDQN in cloud computing, *Appl. Sci.*, **11** (2021), 9360–9360. https://doi.org/10.3390/app11209360
30. Z. Peng, J. Lin, D. Cui, A multi-objective trade-off framework for cloud resource scheduling based on the Deep Q-network algorithm, *Cluster Comput.*, **23** (2020), 2753–2767. https://doi.org/10.1007/s10586-019-03042-9

AIMS Press